# Technique for the $sp^2/sp^3$ characterization of carbon materials: *Ab initio* calculation of near-edge structure in electron-energy-loss spectra

J. T. Titantah and D. Lamoen
*TSM, Department of Physics, University of Antwerp, Groenenborgerlaan 171, 2020 Antwerpen, Belgium*
(Received 20 October 2003; revised manuscript received 1 June 2004; published 31 August 2004)

We describe a technique to determine the $sp^3/sp^2$ ratio of carbon materials which is based on the electron-energy-loss spectroscopy and which uses the theoretical spectrum of graphite obtained from *ab initio* electronic structure calculations. The method relies on the separation of the $\pi^*$ and $\sigma^*$ components of the carbon *K* edge of graphite. The resulting $\pi^*$ spectrum is adopted and assumed to be transferable to other carbon systems given an appropriate parametrization of the broadening. The method is applied on a series of Monte Carlo generated amorphous carbon structures and is shown to be stable over a wide range of the energy windows for which spectral integration is performed. The $sp^3$ fractions obtained using this method are found to be in good agreement with those obtained from a microscopic scheme which uses the $\pi$-orbital axis vector analysis (POAV1). From the electron energy loss calculations on the generated amorphous carbon structures, we conclude that the interchangeable use of coordination number and hybridization state can lead to an underestimation of the $sp^3$ fraction of generated amorphous carbon structures for low and moderate densities. For high densities the coordination method and the POAV1 approach gave the same results. The technique was also applied on a series of spectra of plasma deposited amorphous carbon and was found to be in good agreement with the results obtained from a functional fitting approach.

DOI: 10.1103/PhysRevB.70.075115 PACS number(s): 71.55.Jv, 71.15.Mb, 82.80.Pv, 79.20.Uv

## I. INTRODUCTION

The properties of carbon materials are known to be intricately related to the bonding states of carbon atoms in the material. Carbon bonds predominantly in two ways at moderate and high densities ($\rho \geqslant 2.0$ g/cm$^3$): in $sp^2$ configuration, with carbon bonded to three other atoms in a planar geometry, or in tetrahedral $sp^3$ coordination.

The mechanical, electrical, optical, chemical, and thermoelectric properties of carbon materials are strongly influenced by the proportion of $sp^3$ carbon atoms in the material. Due to their chemical inertness, high hardness and low friction, amorphous carbon finds applications in coating for magnetic storage devices, razor blades, optical devices, field emitting devices, and bio-compatible coating for human inplants (see Ref. 1 and references therein).

Several techniques are often used to deposit amorphous carbon materials. These methods include the use of direct ion beam, arc discharge, laser ablation, sputtering and ion assisted deposition methods.[2] The resulting carbon material can be analyzed for $sp^3$ content using a variety of procedures. Amongst them, the most widely used are the x-ray photoelectron spectroscopy (XPS) (see Ref. 3 and references therein), the plasmon energy technique,[4,5] the near-edge x-ray absorption spectroscopy (NEXAFS)[6] and the high-energy electron-energy-loss spectroscopy (HEELS).[5,7–10] The last two techniques are considered the most reliable.

The high-energy EEL spectrum of an amorphous carbon is made of a $\pi^*$ part whose onset is at about 284 eV and a $\sigma^*$ component whose onset is about 5–7 eV from that of the $\pi^*$ component. The HEELS $sp^3/sp^2$ characterization technique is based on the ability to isolate the $\pi^*$ features and subsequently its cross section from the entire spectrum. All the isolation methods that are often used are limited by the assumption that the $\pi^*$ and the $\sigma^*$ bands are well separated in energy such that their cross sections can be independently deduced by spectral integrations over fixed energy windows. But it is well known that plural inelastic scattering such as core-loss excitation plus additional plasmon losses modifies the edge intensities by redistributing oscillator strengths to higher energies.[8] In particular, for amorphous carbon the $\pi^*$ band can get redistributed to energies as high as 30 eV beyond the edge onset thereby overlapping with the $\sigma^*$ band. Calculations on graphite and amorphous carbon (which will be presented in this paper) reveal that the $\pi^*$ band is exceptionally broad, extending even to energies beyond 30 eV. Also the lifetime broadening of the spectrum which is a function of the energy loss[11,12] will lead to a spread of the $\sigma^*$ intensities to lower energies for which intensities are usually associated to the $\pi^*$ feature.

A straightforward method of $sp^3/sp^2$ quantification is the two energy windows method.[8] The energy windows $\Delta E_\pi$ (for the $\pi^*$ part) and $\Delta E_\sigma$ (for the $\sigma^*$ part) are chosen and located at some convenient points on the spectrum. The spectrum is integrated in each window and the areas in $\Delta E_\pi$ and $\Delta E_\sigma$ are assumed to be entirely due to $1s \rightarrow \pi^*$ and $1s \rightarrow \sigma^*$ transitions, respectively. The ratio of the two areas is compared with a reference ratio and the $sp^3$ fraction is deduced. A problem related to this method is the choice of the widths of these energy windows. It is known that a slight variation of these windows may lead to large variation in the $sp^3$ (or $sp^2$) fraction, e.g., Bruley *et al.*[8] showed that while this ratio depends weakly on the size of the $\sigma^*$ energy window, it depends strongly on the size and position of the $\pi^*$ window.

Another technique of the $\pi^*/\sigma^*$ spectral separation often adopted is the functional fitting technique.[9,13] For this method the spectrum is fitted by a linear combination of

 

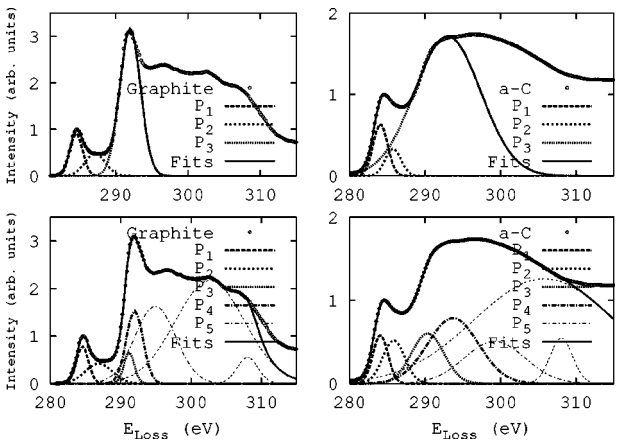


FIG. 1. Functional fitting of measured HEELS of graphite (left panels) and an amorphous carbon sample (right panels). The total spectra, up to 310 eV, may be fitted by a sum of seven Gaussian functions as shown on the lower panels.

Gaussian and/or Lorentzian functions centered on various energy values up to about 10 eV beyond the edge onset (see the upper panels of Fig. 1). Three functions are usually adopted and assigned as follows: the two lowest lying are taken to be the $\pi^*$ features and the highest energy peak taken as the $\sigma^*$ peak. The first peak at about 285 eV is unambiguously a $\pi^*$ peak while the allocation of the second at about 287–288 eV as a $\pi^*$ has been a subject of discussion. It is often said to originate from the $1s \rightarrow \pi^*$ transition for $sp^2$ carbon atoms bonded to hydrogen[14] or from carbon atoms in an intermediate state.[9] We shall demonstrate using calculations on graphite that in addition to the peak at 285 eV the $\pi^*$ spectra of carbon systems are made up of many other peaks at higher energies, the 287–288 peak being one of them. The third peak $P_3$ at about 8 eV above the $\pi^*$ onset is usually assigned as the $\sigma^*$ peak, but we will show that it has a considerable $\pi^*$ contribution. It was recently pointed out[15] that representing the $\sigma^*$ contribution by just one Gaussian function is not sufficient: the 297 eV peak was the dominant contribution to the $\sigma^*$ spectrum rather than the 292 eV peak of the three-functional fitting approach. In fact, on the lower panel of Fig. 1 we show that the energy-loss near-edge structure (ELNES) spectrum, up to 310 eV, may be fitted as a linear combination of an arbitrary number (e.g., seven) Gaussian functions. Higher energy peaks are seen to overlap strongly.

Another drawback of this technique is related to the choice of the energy upper limit $E_{\max}$ for the three-functional fittings. A change in $E_{\max}$ by ±2 eV leads to a huge change in the ratio $\mathrm{Area}(P_1+P_2)/\mathrm{Area}(P_1+P_2+P_3)$ which is usually compared with a reference sample's (e.g., graphite) ratio to get the $sp^3$ fraction. This big change is accompanied by a big change in the $sp^3$ ratio (more than 10%). Table I illustrates this on the amorphous carbon sample obtained from Ref. 16 and whose ELNES spectrum is shown in Fig. 1.

In this paper, we describe a technique of $sp^3/sp^2$ characterization of carbon materials. The method enables a consistent theoretical separation of the $\pi^*$ and $\sigma^*$ features of amorphous carbon based on a first-principles calculation of the ELNES spectrum of graphite. We shall show that this technique avoids most of the problems mentioned above. In particular, it is shown to yield results which are independent of the width of the energy window used for the spectral integration. In Sec. II we summarize the computational method. In Sec. III we present the results for the ELNES of graphite showing how an orientation resolved calculation can lead to the isolation of the $\pi^*$ and $\sigma^*$ features of the spectrum. In order to obtain insight into the local structure of amorphous carbon, we generate eight carbon systems (consisting each of 64 atoms) by classical Monte Carlo techniques and in Sec. IV density functional theory (DFT) calculations are performed on them. The $1s \rightarrow 2p$ ELNES excitation is calculated for these systems. The method of the $sp^3/sp^2$ characterization is described and applied on the generated carbon systems and some plasma deposited samples in Sec. V. A microscopic analysis based on the local bonding structure of every atom of the generated amorphous carbon system provides an alternative method to obtain the $sp^3$ fraction. Section VI summarizes the main results.

TABLE I. The ratios $R=\mathrm{Area}(P_1+P_2)/\mathrm{Area}(P_1+P_2+P_3)$ and the percentages of $sp^3$ carbon. $E_{\max}$ denotes the energy upper limit at which the fitting is limited.

| $E_{\max}$ (eV) | $R$ Sample | $R$ Graphite | $sp^3$ (%) |
|---|---|---|---|
| 291 | 0.210 | 0.333 | 37 |
| 292 | 0.241 | 0.334 | 28 |
| 293 | 0.185 | 0.243 | 24 |

## II. COMPUTATIONAL DETAILS

DFT calculations are performed using the *ab initio* all-electron full-potential-linearized-augmented-plane-wave (FLAPW) package WIEN2k.[17,18] The exchange and correlation energy is treated using the local density approximation[19] which is a fit to the Green's function Monte Carlo calculations of Ceperley and Alder.[20]

For carbon the 1*s* state is the core state while the 2*s* and 2*p* states are the valence states. Muffin-tin radii ($R_{\mathrm{MT}}$) are fixed at 1.3 atomic units (a.u.) for graphite and 1.25 a.u. for amorphous carbon (*a*-C), while $R_{\mathrm{MT}} \times K_{\max}$ values of 5.5 and 5.0 are used for graphite and *a*-C, respectively; $K_{\max}$ being the plane wave cutoff. Calculations with $R_{\mathrm{MT}} \times K_{\max}$ of 5 and 4.5 for graphite and *a*-C showed that these adopted $R_{\mathrm{MT}} \times K_{\max}$ values of 5.5 and 5.0 for graphite and *a*-C, respectively, gave converged ELNES spectra. Up to 1000 *k* points are used to sample the full Brillouin zone of graphite [72 in the irreducible Brillouin zone (IBZ)] while 20 (four in the IBZ) are used for the *a*-C. The core-hole effect is introduced in the ELNES of graphite via the so-called excited-core method in a supercell formulation. For graphite supercells containing 16 atoms (eight atoms per graphene plane) are used. No core-hole calculation is performed on the *a*-C systems. The decomposition of the ELNES of graphite into its

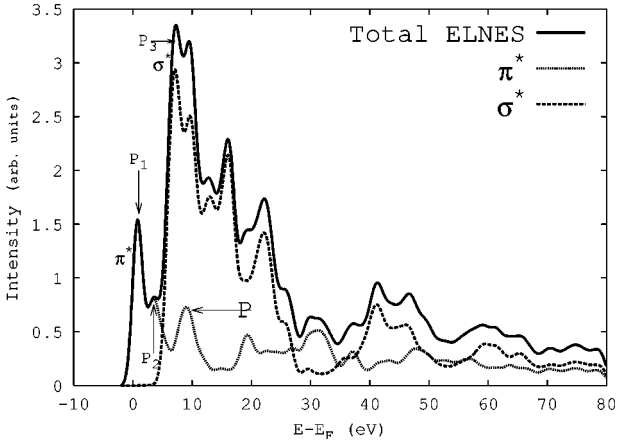


FIG. 2. Calculated C *K* ELNES spectrum of graphite showing $\pi^*$ and $\sigma^*$ and the characters of $P_1$, $P_2$, and $P_3$. The $\pi^*$ component of the spectrum (dotted line) shows a strong feature *P* at about the same energy as the $P_3$ feature.

$\pi^*$ and $\sigma^*$ components is done using the formulation of Nelhiebel *et al.*[21] which has been implemented in the WIEN2k code[17] and applied to hexagonal boron nitride.[22] Recently we performed similar calculations which permitted us to understand the effect of curvature on the anisotropy of carbon nanotubes.[23]

A classical technique was adopted to generate the *a*-C systems. By using the Tersoff empirical potential[24] for carbon,[25] we generate amorphous carbon samples at densities of 2.0, 2.6, 2.8, 3.0, 3.2, 3.4, 3.5, and 3.6 g/cm$^3$ by quenching hot liquid carbon at 5000 K (for the 2.0 g/cm$^3$ carbon) and 8100 K (for higher densities) down to 300 K. This was done via a continuous space, periodic boundary condition (PBC), constant volume, constant temperature, and constant number of atoms classical Metropolis Monte Carlo procedure on cubic cells made of 64 atoms. The atoms were given initial configurations of a simple cubic lattice. The crystal was melted over 100 000 Monte Carlo (MC) steps to form a uniform liquid as the radial distribution function $g(r)$ showed. The system was then quenched exponentially down to 300 K over 320 000 MC moves in 25 steps and then maintained at 300 K for 200 000 MC steps for statistical averaging. We calculate the ELNES spectra, within the DFT approach, of the eight generated amorphous carbon systems.

## III. CALCULATION OF THE ELNES OF GRAPHITE

Orientation resolved ELNES calculations were performed on graphite. The detailed results, reported elsewhere,[26] are in good agreement with HEELS measurements. The result presented here was obtained by adopting the fast electron beam convergence semiangle of 1.87 mrad and the collection semiangle was set to the magic value of 3.01 mrad. This microscope setting was shown[16,26] to yield orientation independent spectra for graphite. In Fig. 2 we show the calculated total ELNES of graphite together with the $\pi^*$ and the $\sigma^*$ components. The energy difference of 6.4 eV between the main $\pi^*$ peak and the $\sigma^*$ peak is in very good agreement with the experimental value of 6–7 eV. The $P_1$, $P_2$, and $P_3$ features of the functional fitting method of $sp^3/sp^2$ characterization is clearly seen. The $\pi^*/\sigma^*$ decomposition reveals clearly that $P_2$ is a $\pi^*$ feature. It also emerges from this figure that the $\pi^*$ component extends to very high energies. In fact, the $\pi^*$ component is nonzero for the entire explored energy range and there is no reason for this to be different for *a*-C systems. A $\pi^*$ peak *P* featuring at about 8 eV from the edge onset and overlapping with the main $\sigma^*$ peak shows that the $P_3$ peak is not entirely of $\sigma^*$ character.

## IV. GENERATED AMORPHOUS CARBON

As described earlier, we performed classical Monte Carlo simulations on eight systems each made of 64 carbon atoms in a cubic box at fix densities of 2.0, 2.6, 2.8, 3.0, 3.2, 3.4, 3.5, and 3.6 g/cm$^3$, respectively. Here we recall that graphite and diamond have a density of about 2.3 and 3.5 g/cm$^3$, respectively. A detailed report on the structural and electronic properties of all the generated systems will be presented elsewhere. In this work we focus on the $sp^3/sp^2$ bonding ratios of the generated carbon systems by exploiting the atomic coordination (which is defined as the number of atoms within a sphere around a given atom as explained in more details later on in this section) and correcting for the nonplanarity of the three-coordinated sites. This is done by using the $\pi$-orbital axis vector (POAV1) analysis[27–29] often used to study the curvature-induced reactivity of fullerenes. We next calculate the average (over all atoms) coreloss spectrum of each of the systems and use them to test for a technique of $sp^3/sp^2$ characterization of amorphous carbon materials.

### A. The $\pi$-orbital axis vector analysis

It is common place to interchangeably use bonding state with coordination number. But the chemistry of curved carbon materials reveals that local configurations play an important role in the bonding state of a carbon atom.[30] While a three-coordinated carbon atom sitting in an ideal trigonal geometry (the atom with its three nearest neighbors sitting in the same plane, all three bond angles equal to 120°, and all three bond lengths equal ~1.4 Å) is known to be in an $sp^2$ bonding state, the deviation from this configuration (for example, by curving the plane of the four atoms as in fullerenes and nanotubes) can lead to a substantial three-dimensional ($sp^3$ character) bonding structure of the three-coordinated atom, making the atom to acquire an intermediate bonding state which can be denoted as $sp^{2+\delta}$. This local distortion can lead to enhanced chemical reactivity of the carbon atoms that participate in the distortion. For instance, the carbon atoms at the cap of carbon nanotubes are known to be more reactive than those along the walls and those of the $C_{60}$ molecule are known to exhibit an $sp^{2.28}$ bonding state, intermediate between ideal two-dimensional $sp^2$ and three-dimensional $sp^3$ bonding states. Because of this the $C_{60}$ molecule shows properties that differ from those of graphite and diamond. Further evidence for distortion-enhanced reactivity is found in a recent simulation study[31] which predicts that the chemisorption of hydrogen atoms to the walls of a (10,10) carbon nanotube

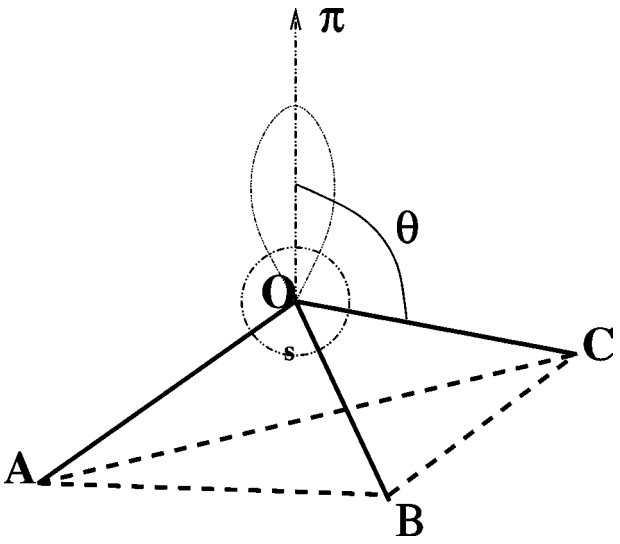


FIG. 3. The pyramidalization of a three-coordinated atom O. $\pi$ is the $\pi$-orbital axis which makes an equal angle with the three bonds OA, OB, and OC. $\gamma=\theta-\pi/2$ is the pyramidalization angle.

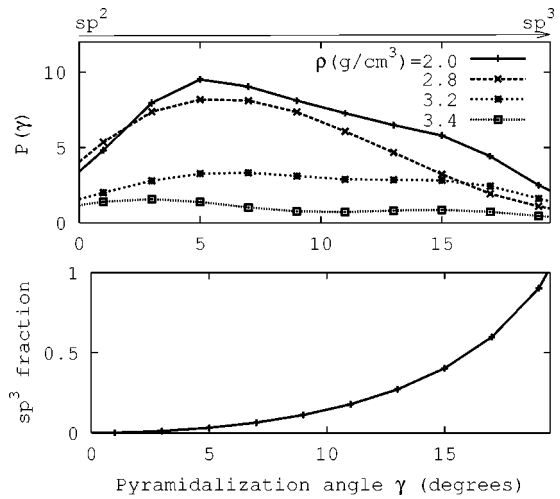


FIG. 4. The distribution of the pyramidalization angle $\gamma$ formed by three coordinated atoms in four amorphous carbon matrices of densities of 2.0, 2.8, 3.2, and 3.4 g/cm$^3$ (upper panel) and the dependence of the $sp^3$ fraction $\delta$ on $\gamma$ [Eq. (3)]. The lines are guides to the eye. The arrow indicates the transition from pure $sp^2$ to $sp^3$ configurations.

can be favored by as much as 1.6 eV at regions of high conformational deformations.

The effect of curvature on the bonding state of a three-coordinated atom in carbon materials has been studied using the $\pi$-orbital axis vector analysis. In this approach the curvature effect is characterized by defining the $\pi$-orbital axis as one making equal angle ($\theta$) with all the three $\sigma$ bonds of the conjugated atom. Figure 3 illustrates the $\pi$-orbital axis of a three-coordinated atom O bonded to atoms A, B, and C. The $\pi$-orbital axis is the axis indicated as $\pi$. For equal bond lengths, it is normal to the plane ABC. $\theta$ is the angle between any of the three bond vectors **OA**, **OB**, and **OC** and this axis. It is given by

$$\cos(\theta) = \frac{(\mathbf{AB}\times\mathbf{AC})\cdot\mathbf{OA}}{|\mathbf{AB}\times\mathbf{AC}||\mathbf{OA}|} = \frac{(\mathbf{AB}\times\mathbf{AC})\cdot\mathbf{OB}}{|\mathbf{AB}\times\mathbf{AC}||\mathbf{OB}|} = \frac{(\mathbf{AB}\times\mathbf{AC})\cdot\mathbf{OC}}{|\mathbf{AB}\times\mathbf{AC}||\mathbf{OC}|}. \quad (1)$$

The pyramidalization angle is defined as the angle $\gamma=\theta-90°$.

Consider the case where atoms O, A, B, and C all lie in the same plane. In this case the $p_z$ and $s$ orbitals do not hybridize. As atom O is lifted out of the plane, a fraction $m$ of the $s$ orbital hybridizes with the $p_z$ orbital to form the $s^m p_z$ hybrid. The remaining fraction 1-$m$ of the $s$ orbital then hybridizes with the $p_x$ and $p_y$ orbitals to form the $s^{1-m}p^2$ orbital which can be rewritten as $sp^{2/(1-m)}$. This new hybrid can be interpreted as $sp_x p_y p_z^{\delta}$, meaning that a fraction $\delta$ of the $p_z$ electrons participate in the $\sigma$-bond formation. $\delta$ is obtained from $m$ as $\delta=2/(1-m)-2$. In the POAV1 analysis $m$ is related to $\theta$ as

$$\frac{m}{m+1} = 2\cot^2\theta. \quad (2)$$

On neglecting the effects of bond-length and bond-angle fluctuations, the fraction of $sp^3$ character ($\delta$) in such a three-coordinated atom is then obtained from $\theta$ as

$$\delta = \frac{4\cot^2\theta}{1-4\cot^2\theta}. \quad (3)$$

In the limit of planar configuration $\theta=90°$ and $\delta=0$ while in the limit of tetragonal configuration $\theta=109.47°$ and $\delta=1$.

For the generated $a$-C systems, we defined the coordination number of an atom as the number of atoms within a sphere of radius $R_c$ centered on the atom. We take $R_c=1.9$ Å, corresponding to a value which lies in a well-defined minimum of the pair correlation function $g(r)$ situated just beyond the shell of the first neighbors. For $R_c$ values varying from 1.8 to 2.0 Å, the coordination numbers of all the generated $a$-C systems were stable. The pyramidalization angles of all the three-coordinated atoms and the corresponding $\delta$'s were calculated. Figure 4 illustrates the distribution of the pyramidalization angle in four amorphous carbon matrices of varying densities together with the dependence of the $sp^3$ fraction $\delta$ of a three-coordinated atom on the pyramidalization angle $\gamma$.

The deviation from ideal tetrahedral structure of the four-coordinated atoms entails some $sp^2$ character that is evidenced from the nonvanishing ELNES intensity close to the edge onset of the $\pi^*$ spectrum. We will show in Sec. V how one must correct for this in the $sp^3$ fraction analysis.

### B. The ELNES spectra of the generated *a*-C structures

DFT calculations were performed on the eight generated $a$-C samples and the carbon 1$s$ electron-energy-loss spectra (EELS) were calculated for all the 64 atoms. For each system the average EEL spectrum was obtained as shown in Fig. 5. All the spectra are shifted vertically for better visualization.

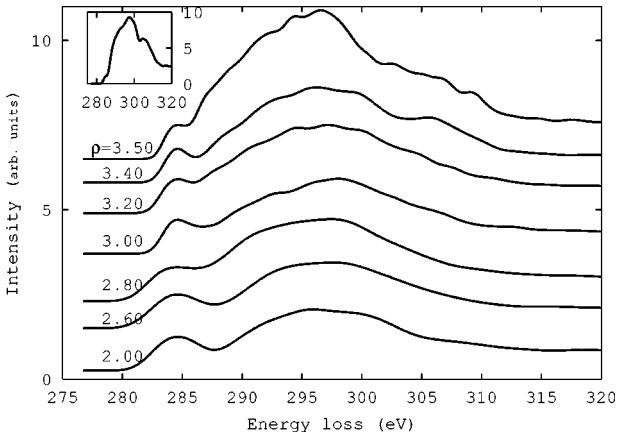


FIG. 5. Average ELNES (in the sudden approximation) of eight MC generated carbon structures of varying densities of 2.00–3.50 g/cm$^3$. All the $\pi^*$ peak maxima are adjusted to lie at 284.6 eV. Along the $y$ axis, intensities are given in arbitrary units and each spectrum is shifted for the purpose of clarity. In the inset we show the ELNES spectrum of the 3.60 g/cm$^3$ system.

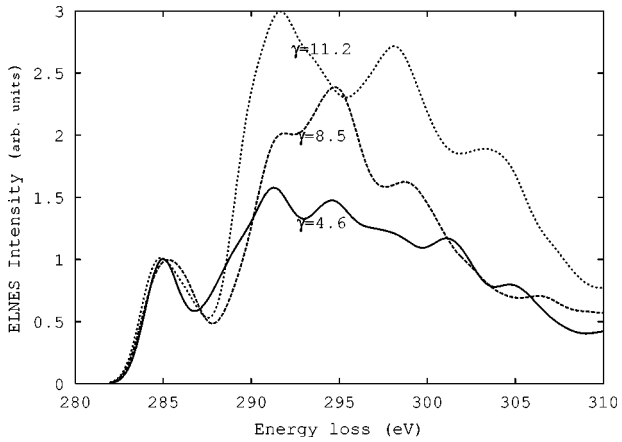


FIG. 6. The ELNES of some three-coordinated atoms with pyramidalization angles $\gamma=4.6°$, 8.5°, and 11.2°, respectively. Remark that as $\gamma$ increases the relative intensity of the $\sigma^*$ to $\pi^*$ increases indicating enhanced three dimensionality.

The spectra are rescaled such that the intensities at the main $\pi^*$ peak are equal to 1. The $\sigma^*$ intensity increases smoothly with increasing density up to 3.5 g/cm$^3$. A huge rise in this intensity is recorded for the highest density case of 3.6 g/cm$^3$ (not shown), which would correspond to a density higher than that of diamond.

The 3.4, 3.5, and 3.6 g/cm$^3$ samples are clearly $sp^3$-rich samples as, apart from the broad $\sigma^*$ edge (a consequence of the disordered structure), new features similar to those of diamond can be seen occuring between 300 and 310 eV. Such features can only be faintly perceived in the lower density systems.

If a three-coordinated atom has a significant proportion of $sp^3$ character this must be translated into the ELNES spectrum as an increase of the intensity of the $\sigma^*$ edge with respect to the $\pi^*$ edge. Since this proportion should increase as the pyramidalization angle increases, the dependence of the relative intensity of the $\sigma^*$ peak to $\pi^*$ peak on this angle should reflect this tendency. Figure 6 clearly confirms this trend. This result reveals that the simple nearest neighbor counting method of the $sp^3$ fraction determination of generated $a$-C systems should yield the lower limit of the latter. By limiting the definition of the $sp^3$ hybridization state to those atoms that are four coordinated, we can understand why most of the reported $sp^3$ fractions of generated $a$-C are often lower than experimental predictions even for $a$-C generated using first-principles techniques.[32] By considering the POAV1 analysis we shall show that the resulting $sp^3$ fraction is consistently higher than the proportion of four-coordinated atoms in generated $a$-C systems for low and intermediate density systems. For higher densities the coordination method predicts the correct $sp^3$ fraction.

The curvature enhanced hybridization of the three-coordinated atoms can be understood as a consequence of the introduction of partial radical character on the $\pi$-bonding electron whose energy increases locally.[31] This radicalization results from reduced spatial overlap of $p$ orbitals that contribute to conjugation in the system. The radical formation is the basis of the heightened reactivity of curved carbon systems.

## V. AN ALTERNATIVE TECHNIQUE FOR THE $sp^3/sp^2$ CHARACTERIZATION OF CARBON MATERIALS

The technique of the $sp^3/sp^2$ characterization presented here is based on the assumption that the ELNES of any carbon atom can be decomposed into two independent parts. One of these ELNES components (the $\pi^*$ component) is sought by performing theoretical calculations on graphite which is a well-known system for which the two components are well defined. The $\pi^*$ spectrum is then assumed to be transferable to other carbon systems given an appropriate parametrization of the broadening. To illustrate this assumption, we performed an orientation resolved ELNES calculation on a three-coordinated atom sitting in a Monte Carlo generated $a$-C matrix in which all its three nearest neighbors were also three coordinated so that a degree of conjugation is guaranteed like in graphite. Figure 7 compares the $\pi^*$ spectrum of carbon in graphite and that of this atom. The two spectra show similar features. The difference between the two spectra evidenced between 5 and 15 eV is a consequence of the large bond-angle fluctuation of $105° \pm 12°$ at this atom.

To some extent, the method described here is comparable to the experimental work of Ref. 33 in which the spectrum of graphite is separated into two independent components with the axis parallel and perpendicular to the beam direction. Our $sp^3/sp^2$ quantification procedure is described as follows:

(i) We identify the energy position $E_\pi$ of the main $\pi^*$ peak from the spectrum of the uncharacterized sample and rescale the intensity to have a value of 1 at this peak. We denote this new spectrum as $I(E)$ where $E$ is the energy loss.

(ii) We consider a normalized smoothing function $g(\sigma, E)$ (which could be a Gaussian or a Lorentzian) of full width at half-maximum $\sigma$.

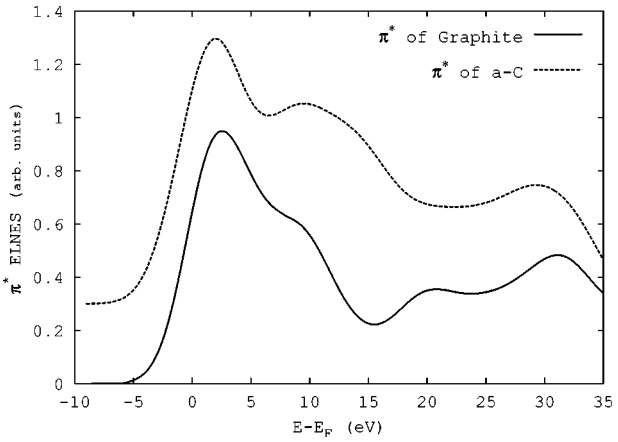


FIG. 7. The $\pi^*$ ELNES components of the carbon $K$ edge of graphite and a three-coordinated atom of an $a$-C system. The three nearest neighbors of this atom are in turn three coordinated.

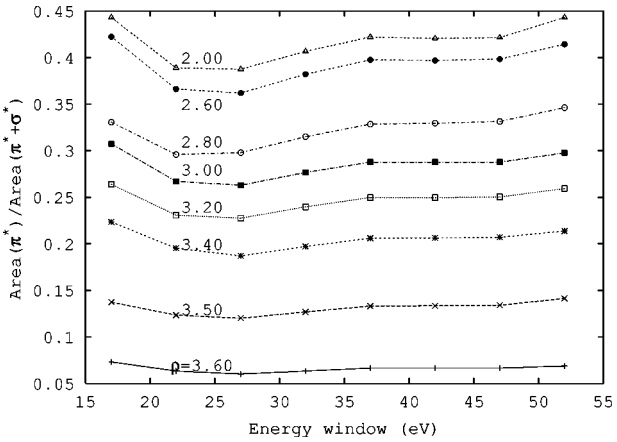


FIG. 9. The ratio $R=\mathrm{Area}(\pi^*)/\mathrm{Area}(\pi^*+\sigma^*)$ for the eight generated carbon structures. Remark that all the lines are approximately parallel to each other.

(iii) We define an energy scale shift parameter $s$ by which the unbroadened calculated graphite $\pi^*$ spectrum should be shifted to align the maximum of its main $\pi^*$ peak to that of the unknown sample. After the spectral shift the $\pi^*$ spectrum is scaled to one at $E_\pi$.

(iv) Using this new shifted graphite $\pi^*$ spectrum which is convolved with $g(\sigma,E)$, and denoted as $\Pi(s,\sigma,E)$, we define the function

$$F(s,\sigma)=\int_{E_{\min}}^{E_\pi}(I(E)-\Pi(s,\sigma,E))^2\,dE, \tag{4}$$

where $E_{\min}$ is the edge onset. In Eq. (4) it is implied that the spectrum of the $a$-C is entirely of $\pi^*$ character up to the main $\pi^*$ peak.

(v) $F$ is minimized for $s$ and $\sigma$. The minimal values of $s$ and $\sigma$ are used for $\Pi(s,\sigma,E)$ to deduce the $\pi^*$ spectrum which best fits the lower energy part of the unknown spectrum. This shifted and convolved $\pi^*$ spectrum is assumed to be that of the unknown $a$-C system. Figure 8 illustrates this procedure on an $a$-C sample. In this case $g$ is taken as a Gaussian function and the minimal $\sigma$ is found to be 1.0 eV with a corresponding $s$ value of 284.2 eV.

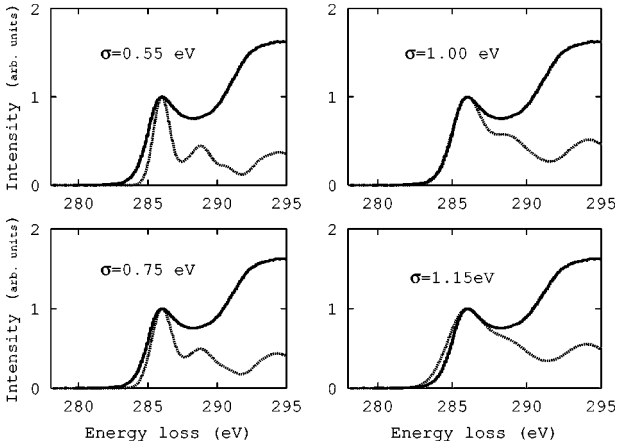


FIG. 8. Matching graphite's calculated $\pi^*$ and measured spectra of an $a$-C sample.

(vi) An energy window $\Delta E$ whose lower limit is fixed at the edge onset is chosen and the integrals $I_\pi(\Delta E)=\int_{E_{\min}}^{E_{\min}+\Delta E}\Pi(s,\sigma,E)dE$ and $I_{\mathrm{Total}}(\Delta E)=\int_{E_{\min}}^{E_{\min}+\Delta E}I(E)dE$ are evaluated.

(vii) The ratios, for various $\Delta E$, $R(\Delta E)=I_\pi(\Delta E)/I_{\mathrm{Total}}(\Delta E)$ are calculated.

(viii) The ratio $R_0(\Delta E)$ for a well-characterized sample, whose $sp^2$ fraction $x_0$ is known, is also calculated and the $sp^2$ fraction in the unknown $a$-C sample is deduced as

$$x(\Delta E)=\frac{R(\Delta E)}{R_0(\Delta E)}x_0 \tag{5}$$

and the $sp^3$ fraction is $1-x$.

To test and validate this method, we applied this technique to the ELNES spectra of the eight generated $a$-C systems described above. The ratio $R(\Delta E)$ for each system is plotted as a function of $\Delta E$ in Fig. 9. From this figure it is seen that for each energy window $R$ decreases monotonically as the density increases. It is also seen that for the wide range of $\Delta E$ considered ($15\ \mathrm{eV}<\Delta E<55\ \mathrm{eV}$) all the curves showing the variation of $R$ with $\Delta E$ seem to be parallel to each other. This means that if one of the spectra was a reference spectrum then the ratio of $sp^2$ carbon in each spectrum with respect to this reference will be fairly constant over this wide energy range. This demonstrates that the method should yield $sp^2$ or $sp^3$ fractions that are independent of the choice of the energy window in contrast to other techniques. In those techniques the $sp^3$ fraction depends crucially on both the width and position of the energy window.

In order to illustrate the method described in this paper, we take one of the Monte Carlo generated amorphous carbon structures as a reference. Because the $sp^3$ fraction determined by the POAV1 analysis coincides with that obtained by the nearest neighbor counting method for high densities,

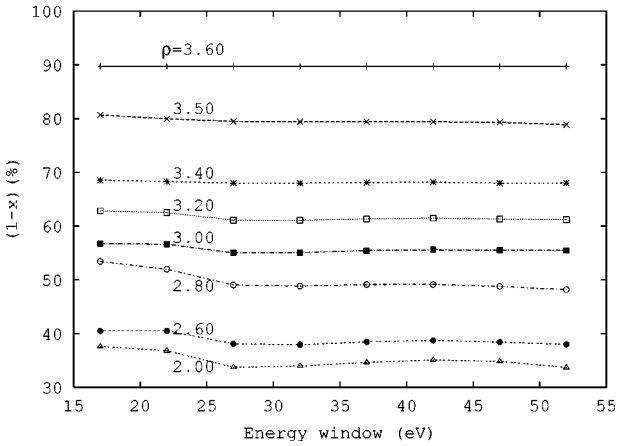


FIG. 10. The $sp^3$ percentage for the eight generated carbon structures. The $\rho=3.6$ g/cm$^3$ sample made of 10.3% $sp^2$ atoms (according to the POAV1 approach) is used as the reference system.

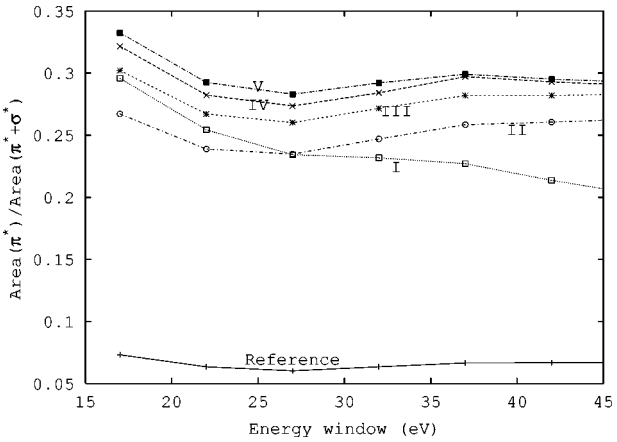


FIG. 11. The ratio $R=\mathrm{Area}(\pi^*)/\mathrm{Area}(\pi^*+\sigma^*)$ for five *a*-C samples. Remark that all the lines are approximately parallel to each other except for sample I.

the structure having a density of 3.6 g/cm$^3$ with an $sp^3$ fraction of 90% is considered as the reference. The resulting fractions for the other six systems are shown in Fig. 10. The $sp^3$ fraction is clearly seen to be independent of the size of the energy window. The largest variation recorded did not exceed 6%. The values obtained, reproduced in Table II were in very good agreement with those obtained using the POAV1 analysis.

*Correcting for $sp^2$ features in two- and four-coordinated atoms*: As pointed out earlier, a plot of the ELNES of some four-coordinated atoms reveals a nonvanishing contribution originating from the transitions into the $\pi^*$ band. This was explained to be a consequence of the deviation from ideal tetrahedral structure through large bond angle and/or bond-length fluctuations. To correct for this bond-fluctuation-induced $sp^2$ character we apply the technique described above as follows. Suppose the $sp^2$ fraction in the system is $x$. Using the ELNES spectrum of each four-coordinated atom, we can isolate the $\pi^*$ component and calculate the average ratio $R$ (over all the four-coordinated atoms), denoted as $R_4$, using the technique. The mean distorsion-induced $sp^2$ fraction in each of the four-coordinated atoms is then $xR_4/R_s$ where $R_s$ is the $R$ ratio for the entire structure. Using the POAV1 analysis we calculate the mean $sp^2$ fraction $x_{\mathrm{POAV}}$ over all the three-coordinated atoms. If we denote the fraction of three-coordinated atoms in the structure as $r_3$ and that of four-coordinated atoms as $r_4$ then $x$ is given by

$$x=\frac{r_3 x_{\mathrm{POAV}}}{1-r_4 R_4/R_s}. \tag{6}$$

Extension to systems containing two-coordinated atoms is straightforward and reads

$$x=\frac{r_3 x_{\mathrm{POAV}}}{1-r_2 R_2/R_s-r_4 R_4/R_s}, \tag{7}$$

where $R_2$ and $r_2$ are the mean (over all two-coordinated atoms) fraction of the $\pi^*$ cross section and the total cross section, and the fraction of two-coordinated atoms in the system, respectively. If there were no two-coordinated atoms on the one hand, and four-coordinated atoms with finite $\pi^*$ ELNES on the other hand, then $R_2=0$ and $R_4=0$, and the $sp^2$ ratio is contributed entirely by three-coordinated atoms as $x=r_3 x_{\mathrm{POAV}}$. If in addition all three-coordinated atoms show local planar structures then $x_{\mathrm{POAV}}=1$ and the $sp^2$ fraction will correspond to the result of the nearest neighbor counting technique. We point out that for structures generated using the Tersoff potential, systems with densities lower than 3.0 g/cm$^3$ contained some two-coordinated atoms ($<10\%$). In Table II, the fourth column includes these $sp^2$ aspects of the two- and four-coordinated atoms. These results are given as intervals because of the standard deviations recorded over the various averages.

Of course, the use of this technique is not restricted to computer generated samples (in contrast to the POAV1 analysis) but can also be applied to experimental spectra. In Fig. 11 we show the $R(\Delta E)$ values for five plasma deposited *a*-C obtained from Ref. 16. Remark that all the curves are

TABLE II. The $sp^3$ percentages of the eight generated amorphous carbon systems as obtained from our alternative method (method I), the coordination method (method II) and the POAV1 analysis (method III), respectively. The 3.6 g/cm$^3$ computer–generated system is considered as reference and its $sp^2$ ratio (0.103) according to the POAV1 is adopted. The results obtained using method I are given as intervals in order to demonstrate the spread over the entire range of the energy window of 15–45 eV.

| Density (g/cm$^3$) | Method I (%) | Method II (%) | Method III (%) |
|---|---|---|---|
| 2.00 | 32–38 | 16 | 28–32 |
| 2.60 | 39–40 | 20 | 35–37 |
| 2.80 | 48–52 | 34 | 46–50 |
| 3.00 | 56–58 | 55 | 54–56 |
| 3.20 | 61–62 | 60 | 60–65 |
| 3.40 | 69–70 | 72 | 68–74 |
| 3.50 | 79–81 | 84 | 81–87 |
| 3.60 | 90 | 90 | 90 |

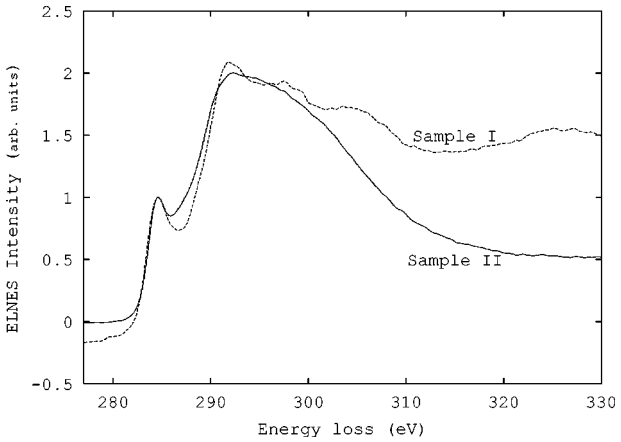


FIG. 12. The rescaled (rescaled to 1 at the main $\pi^*$ peak) spectra of samples I and II showing possible background subtraction problem in sample I.

approximately parallel except for sample I. A possible explanation for this deviation could be a poor spectral treatment (correcting for multiple scattering and background subtraction). This is confirmed from the plot of the rescaled spectra of samples I and II in Fig. 12 where it is clearly seen that sample I is not flat before the edge onset which is an indication of poor background subtraction which could be worse for higher energies. In this way, this technique can also be used to test for the correctness of spectral treatment before quantification. Poor spectral treatment can lead to $sp^3$ fractions that are off their true values by more than 15% of the correct values. As a reference we still retain the MC generated structure of 3.6 g/cm$^3$. The results for the $sp^3$ fraction are shown in Fig. 13 and in Table III. In this table we also listed the values obtained in Ref. 16 using the functional fitting method with three Gaussians.

## VI. SUMMARY

We have developed a method to quantify the $sp^3$ fraction of an amorphous carbon sample based on the theoretical separation of the $\pi^*$ and $\sigma^*$ components of the carbon 1*s* electron-energy-loss spectra.

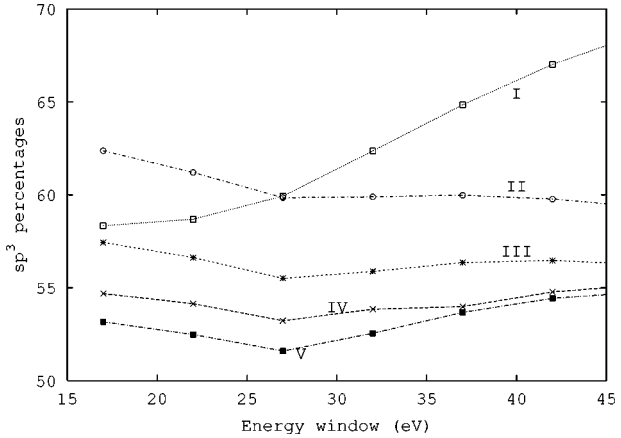


FIG. 13. The $sp^3$ percentage for the five *a*-C samples.

TABLE III. The $sp^3$ percentages of the five *a*-C samples obtained using our technique (method I) and the functional fitting technique. The 3.6 g/cm$^3$ system is considered as reference and its $sp^2$ ratio (0.103) according to the POAV1 is adopted. Apart from sample I, all samples show excellently stable results within the 30 window. The results obtained using method I are given as intervals in order to demonstrate the spread over the entire range of the energy window.

| Sample No. | Method I (%) | Fitting technique (%) |
|---|---|---|
| I | 58–68 | 67–68 |
| II | 60–63 | 61 |
| III | 56–57 | 56 |
| IV | 54–55 | 51–53 |
| V | 52–55 | 53 |

Momentum transfer orientation resolved energy-loss near-edge structure calculations have permitted the isolation of the $\pi^*$ components of the carbon *K* edge in graphite and of an atom of an amorphous carbon system. The $\pi^*$ spectrum of the three-coordinated atom bonded to three other three-coordinated atoms in the amorphous matrix is shown to have similar features as that of graphite.

The $sp^3$ fraction of an amorphous carbon sample is determined from its energy-loss near-edge structure by using the first-principles electronic structure calculation of the energy-loss near-edge structure of graphite. The $\pi^*$ spectrum of graphite is adopted and assumed to be transferable to other carbon systems given an appropriate parametrization of the broadening. This has enabled the isolation of the $\pi^*$ spectrum of the carbon systems and a subsequent characterization of their $sp^3$ contents.

We have applied the method to some Monte Carlo generated amorphous carbon structures and shown that the method gives stable results over a wide range of the energy window used for spectral integration and that their $sp^3$ fractions obtained using this method agree with values obtained using the $\pi$-orbital axis vector analysis. The method has also been applied to five amorphous carbon samples and found that this method yields results that compare well with the functional fitting method. In sharp contrast with conventional techniques, we have demonstrated that the proposed method is independent of the choice of the energy window used for the spectral integration.

Also, we have shown that the POAV1 analysis can be applied to generated amorphous carbon systems to predict the correct bonding structures. This can lead to an up-grade of the $sp^3$-bonding fraction of low and intermediate density carbon as compared to the prediction of the simple coordination number. We have, therefore, found that for low and moderate density generated amorphous carbon, the interchangeable use of coordination number and hybridization state can lead to an underestimation of the $sp^3$ fraction of generated amorphous carbon. It emerges from this study that computer-generated amorphous carbon structures can be used to quantify real carbon materials, on the condition that the bonding structure of the former is well characterized.

**ACKNOWLEDGMENTS**

The authors would like to thank the authors of Ref. 16 for providing their data and K. Jorissen, A.-L. Hamon, J. Verbeeck, D. Schryvers, and P. Potapov for stimulating discussions. Part of this work was supported by the Special Research fund of the University of Antwerp (BOF-NOI) and a GOA from the University of Antwerp "Characterization of nano-structures by means of advanced electron energy spectroscopy and filtering."

[1] A. Grill, Diamond Relat. Mater. **8**, 428 (1999).
[2] Y. Lifshitz, Diamond Relat. Mater. **8**, 1659 (1999).
[3] R. Haerle, E. Riedo, A. Pasquarello, and A. Baldereschi, Phys. Rev. B **65**, 045101 (2001).
[4] R. F. Egerton, *Electron Energy-loss Spectroscopy in the Electron Microscope* (Plenum, New York, 1986).
[5] A. C. Ferrari, A. Libassi, B. K. Tanner, V. Stolojan, J. Yuan, L. M. Brown, S. E. Rodil, B. Kleinsorge, and J. Robertson, Phys. Rev. B **62**, 11 089 (2000).
[6] G. Comelli, J. Stöhr, C. J. Robinson, and W. Jark, Phys. Rev. B **38**, 7511 (1988).
[7] P. J. Fallon, V. S. Veerasamy, C. A. Davis, J. Robertson, G. A. J. Amaratunga, W. I. Milne, and J. Koskinen, Phys. Rev. B **48**, 4777 (1993).
[8] J. Bruley, D. B. Williams, J. J. Cuomo, and P. Pappas, J. Microsc. **180**, 22 (1995).
[9] A. J. Papworth, C. J. Kiely, A. P. Burden, S. R. P. Silva, and G. A. J. Amaratunga, Phys. Rev. B **62**, 12 628 (2000).
[10] S. D. Berger, D. R. McKenzie, and P. J. Martin, Philos. Mag. Lett. **57**, 285 (1988).
[11] G. Moos, C. Gahl, R. Fasel, M. Wolf, and T. Hertel, Phys. Rev. Lett. **87**, 267402 (2001).
[12] S. Xu, J. Cao, C. C. Miller, D. A. Mantell, R. J. D. Miller, and Y. Gao, Phys. Rev. Lett. **76**, 483 (1996).
[13] L. Wan, and R. F. Egerton, Thin Solid Films **279**, 34 (1996).
[14] S. R. P. Silva, J. Robertson, Rusli, G. A. J. Amaratunga, and J. Schwan, Philos. Mag. B **74**, 369 (1996).
[15] J. Díaz, S. Anders, X. Zhou, E. J. Moler, S. A. Kellar, and Z. Hussain, Phys. Rev. B **64**, 125204 (2001).
[16] A.-L. Hamon, J. Verbeeck, D. Schryvers, J. Benedikt, and Richard M.C.M. v.d. Sanden, J. Mater. Chem. **14**, 2030 (2004).
[17] P. Blaha, K. Schwarz, G. K. H. Madsen, D. Kvasnicka, and J. Luitz, *WIEN2k, An Augmented Plane Wave + Local Orbitals Program for Calculating Crystal Properties* (Karlheinz Schwarz, Techn. Universität Wien, Austria, 2001).
[18] K. Schwarz, J. Solid State Chem. **176**, 319 (2003).
[19] J. P. Perdew and Y. Wang, Phys. Rev. B **45**, 13 244 (1992).
[20] D. M. Ceperley and B. J. Alder, Phys. Rev. Lett. **45**, 566 (1980).
[21] M. Nelhiebel, P.-H. Louf, P. Schattschneider, P. Blaha, K. Schwarz, and B. Jouffrey, Phys. Rev. B **59**, 12 807 (1999).
[22] C. Hébert-Souche, P.-H. Louf, M. Nelhiebel, J. Luitz, P. Schattschneider, K. Schwarz, and B. Jouffrey, Ultramicroscopy **83**, 9 (2000).
[23] J. T. Titantah, K. Jorissen, and D. Lamoen, Phys. Rev. B **69**, 125406 (2004).
[24] J. Tersoff, Phys. Rev. B **38**, 9902 (1988).
[25] J. Tersoff, Phys. Rev. Lett. **61**, 2879 (1988).
[26] J. T. Titantah and D. Lamoen (unpublished).
[27] R. C. Haddon, Acc. Chem. Res. **21**, 243 (1988).
[28] R. C. Haddon and L. T. Scott, Pure Appl. Chem. **58**, 137 (1986).
[29] R. C. Haddon, J. Am. Chem. Soc. **109**, 2837 (1986).
[30] R. C. Haddon and S. Y. Chow, Pure Appl. Chem. **71**, 289 (1999).
[31] D. Srivastava, D. W. Brenner, J. D. Schall, K. D. Ausman, M. Yu, and R. S. Ruoff, J. Phys. Chem. B **103**, 4330 (1999).
[32] N. A. Marks, N. C. Cooper, D. R. McKenzie, D. G. McCulloch, P. Bath, and S. P. Russo, Phys. Rev. B **65**, 075411 (2002).
[33] N. D. Browning, J. Yuan, and L. M. Brown, Ultramicroscopy **38**, 291 (1991).